ASC Report No. 3/2016

ALmost EXact boundary conditions for transient Schrödinger-Poisson systems

L. Bian, G. Pang, S. Tang, A. Arnold

Institute for Analysis and Scientific Computing —
Vienna University of Technology — TU Wien
www.asc.tuwien.ac.at ISBN 978-3-902627-05-6

Most recent ASC Reports

2/2016 *A. Jüngel and N. Zamponi*
A cross-diffusion system derived from a Fokker-Planck equation with partial averaging

1/2016 *M. Kaltenbäck*
Definitizability of normal operators on Krein spaces and their functional calculus

41/2015 *W. Auzinger, O. Koch, B.K. Muite, M. Quell*
Adaptive high-order splitting methods for systems of nonlinear evolution equations with periodic boundary conditions

40/2015 *W. Auzinger, T. Kassebacher, O. Koch and M. Thalhammer*
Convergence of a strang splitting
finite element discretization for the Schrödinger-Poisson equation

39/2015 *T. Apel, J.M. Melenk*
Interpolation and quasi-interpolation in
h- and hp-version finite element spaces (extended version)

38/2015 *H. Woraceki*
xxxx

37/2015 *A. Jüngel and N. Zamponi*
Quality behavior of solutions to cross-diffusion systems from population dynamics

36/2015 *A. Jüngel and W. Yue*
Discrete Beckner inequalities via the Bochner-Bakry-Emery approach for Markov chains

35/2015 *J. Burkotová, I. Rachunková, M. Hubner, E. Weinmüller*
Numerical evidence of Kneser solutions to a class of singular BVPs in ODEs.

34/2015 *O. Koch, S. Schirnhofer, E. Weinmüller*
Numerical simulation of the Korteweg-
de Vries Equation for shallow water waves.

Institute for Analysis and Scientific Computing
Vienna University of Technology
Wiedner Hauptstraße 8–10
1040 Wien, Austria

E-Mail: admin@asc.tuwien.ac.at
WWW: http://www.asc.tuwien.ac.at
FAX: +43-1-58801-10196

ISBN 978-3-902627-05-6

© Alle Rechte vorbehalten. Nachdruck nur mit Genehmigung des Autors.

ALmost EXact boundary conditions for transient Schrödinger-Poisson system

Lei Bian[a], Gang Pang[b], Shaoqiang Tang[a,*], Anton Arnold[c]

[a]*HEDPS, CAPT, College of Engineering, Peking University, Beijing 100871, China*
[b]*Institute of Applied Physics and Computational Mathematics, Beijing 100088, China*
[c]*Institut für Analysis und Scientific Computing, TU-Wien, Wiedner Hauptstr. 8, 1040 Wien, Austria*

Abstract

For the Schrödinger-Poisson system, we propose an ALmost EXact(ALEX) boundary condition to treat accurately the numerical boundaries. Being local in both space and time, the ALEX boundary conditions are demonstrated to be effective in suppressing spurious numerical reflections. Together with the Crank-Nicolson scheme, we simulate a resonant tunneling diode. The algorithm produces numerical results in excellent agreement with those in Mennemann et al. [1], yet at a much reduced complexity. The modulus of the wave function exhibits pronounced peaks at resonant values for the wave number. Hence, it is important to incorporate these modes when selecting the cut-off wave number for numerical simulations.

Keywords: Schrödinger-Poisson simulation, ALEX boundary condition, resonant tunneling diode, primary peak, resonant wave numbers

1. Introduction

The Schrödinger-Poisson equations govern many important physical systems, such as the quantum many body system, time-dependent density functional theory, and quantum charge transport in semiconductor devices [1][2][3]. One major challenge in numerical simulations of these equations is a broad band of present wave-numbers that require to be well resolved to reproduce the correct physics. This leads to a huge system coupled through the electron density and self-consistent potential. When resolving each discrete wave number, we need to treat the numerical boundaries in an effective way to suppress non-physical reflections. Otherwise, wrong physics and even numerical instability will destroy the whole simulation.

In the literature, various boundary treatments were developed over the past two decades. An accurate approach is of Dirichlet-to-Neumann (DtN) or Neumann-to-Dirichlet (NtD) type [4][5]. As convolutions are involved, the boundary treatment is rather expensive numerically. Also, it does not apply to nonlinear problems in general. On the other hand, the perfectly match layer (PML) approach applies to quite general systems including the Schrödinger-Poisson system with

*Corresponding author
Email addresses: bianlei@pku.edu.cn (Lei Bian), 1517191281@qq.com (Gang Pang), maotang@pku.edu.cn (Shaoqiang Tang), anton.arnold@tuwien.ac.at (Anton Arnold)

a rather empirical choice of parameters [6][7]. For an overview of several approaches we refer to [8].

In the study of accurate numerical boundary treatments for crystalline solids, we have discovered that the Bessel functions of the first kind satisfy approximate linear relations to any required accuracy [9]. This allows us to design an ALmost EXact(ALEX) boundary condition that works very well in that application. The time history kernel functions of the semi-discretized Schrödinger equation are also based on the Bessel functions. Therefore, we constructed an ALEX boundary condition for the Schrödinger equation, and demonstrated its high efficiency in both linear and nonlinear systems [10]. This boundary condition is local in both space and time, with precomputed coefficients. In this work, we extend the ALEX boundary conditions to the Schrödinger-Possion system, and demonstrate its effectiveness in numerical simulations of a resonant tunneling diode. There we observe quantum resonance at two pronounced values of the wave number: $\pm k_{res}$. In the spatial variable, the two corresponding primary peaks of the wave function appear inside the potential well. In numerical simulations, they contribute substantially to the electron density and hence the self-consistent potential. Accordingly, we propose to account for the quantum resonance in selecting the cut-off wave number sufficiently large to include the two primary peaks.

The rest of this paper is organised as follows. In Section 2, we describe the governing equations for both the stationary and the transient problem. The former is adopted for preparing the initial data for a transient simulation at zero applied voltage, in order to avoid an initial layer. Then in Section 3, we describe the numerical algorithms for both simulations. In particular, we provide the ALEX boundary conditions and the two-way boundary conditions. Numerical tests for a resonant tunneling diode are presented in Section 4. We explore the primary peaks in Section 5. Finally, we make some concluding remarks in Section 6.

2. Governing equations

In this section, we first describe the transient system which governs the dynamics of ballistic charge transport in a resonant tunneling diode. The initial data for this transient system are prescribed by the solution to the corresponding stationary system. The boundary conditions are also given.

2.1. Transient Schrödinger-Poisson system

In a resonant tunneling diode of length L, the electron wave function $\psi(x, k, t)$ at a fixed wave number k is described by the Schrödinger equation

$$i\hbar\psi_t = -\frac{\hbar^2}{2m}\psi_{xx} + V(x,t)\psi, \quad x \in \mathbb{R}, \quad k \in \mathbb{R}, \quad t > 0. \tag{1}$$

Since the wave number does not appear explicitly in the equation, we may solve for each k separately. Here $\hbar$ is the reduced Planck constant, and m is the electron mass. The potential energy $V(x, t)$ consists of two parts, a self-consistent potential energy $V^s(x, t)$ and a built-in barrier potential energy $V^B(x)$ for a resonant tunneling diode. The latter is compactly supported within the device. In particular, the potential outside of the device is assumed to be

$$V(x,t) = \begin{cases} 0, & x \le 0; \\ -eU(t), & x \ge L, \end{cases} \tag{2}$$

where $U(t)$ is a given applied voltage, and e represents the elementary charge. To avoid confusion, throughout this paper we use "exp" to denote the exponential function.

For this (constant-in-x) potential, the Schrödinger equation (1) admits special solutions in the form of plane waves outside of the space interval $[0, L]$. In particular, for $k > 0$, a right traveling plane wave takes the form of

$$\psi^r(x,k,t) = \exp\left(-i\frac{E(k)t}{\hbar} + ikx\right), \quad x \le 0, \tag{3}$$

with $E(k) = \dfrac{\hbar^2 k^2}{2m}$. The reflected wave $\psi(x,k,t) - \psi^r(x,k,t)$ for $x \le 0$ and the transmitted wave $\psi(x,k,t)$ for $x \ge L$ are determined by the potential energy inside the device and the initial data.

For $k < 0$, $x \ge L$, we make the time-dependent transform

$$\tilde{\psi}(x,k,t) = \psi(x,k,t)\exp\left(-\frac{ie}{\hbar}\int_0^t U(s)ds\right). \tag{4}$$

It is straightforward to find that $\tilde{\psi}(x,k,t)$ satisfies the free Schrödinger equation

$$i\hbar\tilde{\psi}_t = -\frac{\hbar^2}{2m}\psi_{xx}, \quad x \ge L, k < 0, t > 0. \tag{5}$$

A left traveling plane wave takes the form of

$$\tilde{\psi}^l(x,k,t) = \exp\left(-i\frac{E(k)t}{\hbar} + ikx\right), \quad x \ge L. \tag{6}$$

Here $E(k) = \dfrac{\hbar^2 k^2}{2m}$. Back to the original wave function $\psi(x,k,t)$, the left traveling plane wave is

$$\psi^l(x,k,t) = \exp\left(-i\frac{(E(k)t - e\int_0^t U(s)ds)}{\hbar} + ikx\right), \quad x \ge L. \tag{7}$$

Again, the transmitted wave $\psi(x,k,t)$ for $x \le 0$ and the reflected wave $\psi(x,k,t) - \psi^l(x,k,t)$ for $x \ge L$ are out-going waves, and satisfy transparent boundary conditions at $x = 0$ and $x = L$, respectively. We remark that these plane waves are bounded in $L^\infty(\mathbb{R})$, but not in $L^2(\mathbb{R})$.

The electron density is calculated as

$$n(x,t) = \int_{\mathbb{R}} g(k)\,|\psi(x,k,t)|^2\,dk, \quad x \in \mathbb{R}, \tag{8}$$

with an injection profile given by the Fermi-Dirac statistics

$$g(k) = \frac{mk_BT_0}{2\pi^2\hbar^2}\ln\left[1 + \exp\left(\frac{E_F - \hbar^2k^2/(2m)}{k_BT_0}\right)\right], \quad k \in \mathbb{R}. \tag{9}$$

Here k_B is the Boltzmann constant, T_0 is the electron temperature, and E_F is the Fermi energy. We remark that the plane waves may be regarded as injected from $x = \pm\infty$, hence $g(k)$ is called the injection profile.

The self-consistent potential energy $V^s(x,t)$ is coupled with the electron density by the Poisson equation in the device.

$$-\varepsilon\frac{\partial^2 V^s}{\partial x^2} = e^2(n(x,t) - n_D(x)), \quad x \in [0,L]. \tag{10}$$

The permittivity ε and doping profile $n_D(x)$ are a given constant and function, respectively. We notice that $V^s(x,t) = V(x,t)$ outside of the device, given by (2). The boundary conditions are therefore given by the continuity of the potential at $x = 0, L$.

Instead of simulating the whole spatial domain $\mathbb{R}$, we perform numerical studies only over the device for $x \in [0,L]$, $k \in [-k_M, k_M]$ with a suitable cut-off wave number k_M, and $t > 0$. Accordingly, we need to impose suitable initial and boundary conditions for the Schrödinger equation (1).

2.2. *Initial data via a stationary Schrödinger-Poisson system*

It is known that quantum device simulations require well-prepared initial data to avoid a strong initial layer [11][12]. Following [1], we shall use the stationary solution $\varphi(x,k)$ as the initial data $\psi(x,k,0)$ for $x \in [0,L]$. Furthermore, in this study we shall take $U(0) = 0$ for the transient simulation.

With an energy $E(k) = \dfrac{\hbar^2 k^2}{2m}$, the wave function $\varphi(x,k)$ and the stationary self-consistent potential $\overline{V}^s$ solve the following equations for each fixed $k \in \mathbb{R}$,

$$E(k)\varphi = -\frac{\hbar^2}{2m}\varphi_{xx} + [V^B(x) + \overline{V}^s(x)]\varphi, \quad x \in [0,L]; \tag{11}$$

$$-\varepsilon\frac{d^2\overline{V}^s}{dx^2} = e^2(\overline{n}(x) - n_D(x)), \quad x \in [0,L]. \tag{12}$$

Here $\overline{n}(x) = \int_{\mathbb{R}} g(k)\,|\varphi(x,k)|^2\,dk$ is the electron density. The boundary conditions for the Poisson equation are

$$\overline{V}^s(0) = \overline{V}^s(L) = 0. \tag{13}$$

Following [6][13], the open boundary conditions for the stationary Schrödinger equation (11) are as follows.

$$\varphi_x(0,k) + ik\varphi(0,k) = 2ik, \quad \varphi_x(L,k) = ik\varphi(L,k), \quad k > 0, \tag{14}$$

$$\varphi_x(0,k) = ik\varphi(0,k), \quad \varphi_x(L,k) + ik\varphi(L,k) = 2ike^{ikL}, \quad k < 0. \tag{15}$$

2.3. *Boundary conditions*

On the boundaries of the device, incoming waves enter from $x = 0$ for $k > 0$, and from $x = L$ for $k < 0$. For $k > 0$, the reflected wave $\psi(x,k,t) - \exp(-i\frac{E(k)}{\hbar}t + ikx)$ for $x \le 0$ satisfies a transparent boundary condition at $x = 0$, and the transmitted wave $\psi(x,k,t)$ for $x \ge L$ satisfies a transparent boundary condition at $x = L$ [14][15]. We remark that depending on the formulation of the used transparent boundary condition, one may have to require consistency between the initial and boundary data [14]. At the right boundary, e.g., $\psi(\cdot,k,0)$ may have to vanish in a neighborhood of $x = L$.

In the same way, for $k < 0$, the transmitted wave $\psi(x,k,t)$ for $x \le 0$ and the reflected wave $\psi(x,k,t) - \exp\left(-i\dfrac{E(k)t - e\int_0^t U(s)ds}{\hbar} + ikx\right)$ for $x \ge L$ satisfy transparent boundary conditions for outgoing waves at $x = 0$ and L, respectively.

We remark that in the literature, there are several numerically effective ways to impose such transparent boundary conditions, and considerable efforts have been put in this important yet difficult topic [7][16][17][18][19].

3. Numerical method

In this section, we first briefly describe the Gummel iteration method for solving the stationary Schrödinger-Poisson system [1]. Then we present the discretization and boundary treatment for the transient problem, along with a sketch of the algorithm.

3.1. Stationary Schrödinger-Poisson system

We discretize the space x and the wave number k with equidistant grids. Let $x_j = j\Delta x$, for $j = 0,\dots,J$ with $x_J = L$; and $k_l = l\Delta k$, for $l = -M,\dots,-1,1,\dots M$, with $k_M = \sqrt{2m(E_F + 7k_BT_0)}/\hbar$. Here the choice of the cut-off wave number follows that in [15][1], which is empirical. Note that we omit here the grid point $k = 0$, since the Schrödinger operator on the right hand side of (11) does not have a zero eigenvalue (remember $E(0) = 0$) for potentials $V(x) \ge 0$ (see Fig. 6). Hence, the initial condition $\varphi(\cdot,0) \equiv 0$ implies $\psi(\cdot,0,\cdot) \equiv 0$.

The equations (11) and (12) are iteratively solved for each $k = k_l$ as follows, with p counting the iteration step, and $\varphi_{j,l} \approx \varphi(x_j,k_l)$, $\overline{V}_j \approx \overline{V}^s(x_j)$, $\overline{n}_j \approx \overline{n}(x_j)$,

$$E^d(k_l)\varphi_{j,l}^{(p)} = -\frac{\hbar^2}{2m(\Delta x)^2}(\varphi_{j+1,l}^{(p)} - 2\varphi_{j,l}^{(p)} + \varphi_{j-1,l}^{(p)}) + [V^B(x_j) + \overline{V}_j^p]\varphi_{j,l}^{(p)}, \tag{16}$$

$$-\frac{\varepsilon}{(\Delta x)^2}(\overline{V}_{j-1}^{(p+1)} - 2\overline{V}_j^{(p+1)} + \overline{V}_{j+1}^{(p+1)}) = e^2\left[\overline{n}_j^{(p)}\exp\left(\frac{\overline{V}_j^{(p)} - \overline{V}_j^{(p+1)}}{V^{ref}}\right) - n_D(x_j)\right]. \tag{17}$$

Here $E^d(k) = \frac{\hbar^2}{m(\Delta x)^2}(1-\cos(k\Delta x))$ is the dispersion relation for the second order finite difference, $V^{ref} = 0.03$eV is a relaxation parameter, and the electron density is calculated from

$$\overline{n}_j^{(p)} = \Delta k\sum_{|l|=1}^{M} g(k_l)\left|\varphi_{j,l}^{(p)}\right|^2. \tag{18}$$

Following [1][14], we take discrete transparent boundary conditions for (16) as follows,

$$-\frac{1}{\alpha^+}\varphi_{-1,l}^{(p)} + \varphi_{0,l}^{(p)} = 1 - \frac{1}{(\alpha^+)^2}, \quad \varphi_{J,l}^{(p)} - \frac{1}{\alpha^+}\varphi_{J+1,l}^{(p)} = 0, \quad k > 0, \tag{19}$$

$$\varphi_{0,l}^{(p)} - \alpha^-\varphi_{-1,l}^{(p)} = 0, \quad \varphi_{J,l}^{(p)} - \frac{1}{\alpha^-}\varphi_{J+1,l}^{(p)} = \left(\frac{1}{\alpha^-}\right)^J - \left(\frac{1}{\alpha^-}\right)^{J+2}, \quad k < 0, \tag{20}$$

with

$$\alpha^\pm = 1 - \frac{mE^d(k)(\Delta x)^2}{\hbar^2} \pm i\sqrt{\frac{2mE^d(k)(\Delta x)^2}{\hbar^2} - \frac{m^2(E^d(k))^2(\Delta x)^4}{\hbar^4}}. \tag{21}$$

The boundary conditions for (17) are homogeneous $\overline{V}_0^{(p+1)} = \overline{V}_J^{(p+1)} = 0$.

3.2. Transient Schrödinger-Poisson system

For the transient problem, the discretized Poisson equation is

$$-\frac{\varepsilon}{(\Delta x)^2}(V_{j-1}^s - 2V_j^s + V_{j+1}^s) = e^2(n_j(t) - n_D(x_j)), \quad j = 1, \ldots, J-1, \tag{22}$$

with $V_0^s = 0$ and $V_J^s(t) = -eU(t)$. Here the electron density is calculated from

$$n_j(t) = \Delta k \sum_{|l|=1}^{M} g(k_l) \left|\psi_{j,l}(t)\right|^2. \tag{23}$$

The Schrödinger equation is semi-discretized in space as

$$i\hbar\frac{d}{dt}\psi_{j,l} = -\frac{\hbar^2}{2m(\Delta x)^2}(\psi_{j+1,l} - 2\psi_{j,l} + \psi_{j-1,l}) + V_j\psi_{j,l}, \quad j \in \mathbb{Z}, \tag{24}$$

with $V_j = V_j^s + V^B(x_j)$.

In the previous work [10], we have discovered that the semi-discretized system (24) admits a time history kernel function (lattice Green's function) in the form of Bessel functions. That is, as $V_j = 0$ for $j \le 0$ in (24) along with the initial condition $\psi_{q,l}(0) = 0$ for $q < 0, 1 \le |l| \le M$, we have

$$\psi_{-q,l}(t) = \frac{q}{t} i^q \exp(-2it) J_q\left(\frac{\hbar t}{m(\Delta x)^2}\right) * \psi_{0,l}(t), \quad t > 0. \tag{25}$$

Meanwhile, through an asymptotic expansion it was discovered that Bessel functions of the first kind are approximately linearly dependent to any required accuracy, provided their orders are big enough [9]. More precisely, for $M_q \ge 5$ and any given $\varepsilon > 0$, if $Q \in \mathbb{N}$ is big enough, there exist a set of real numbers a_q $(1 \le q \le M_q)$, such that

$$\left|\sum_{q=1}^{M_q} a_q J_{Q-q}(t) - J_Q(t)\right| < \frac{\varepsilon}{\sqrt[3]{Q}}, \quad \forall t \ge 0. \tag{26}$$

This naturally yields a transparent boundary condition

$$\psi_{-Q,l}(t) \approx \sum_{q=1}^{M_q} a_q \psi_{-Q+q,l}(t), \quad t \ge 0. \tag{27}$$

Using the recursive relation for the derivative of the Bessel functions, we may further enhance the efficiency for numerical boundary treatments. After some calculations, the approximate linear dependency leads to an ALmost EXact (ALEX) boundary condition as follows [10]:

$$i\hbar\frac{d}{dt}\psi_{-Q,l} = \sum_{q=0}^{M_q} b_q \psi_{-Q+q,l}. \tag{28}$$

In this study, we take the same formulation as in [10] with $M_q = 15$ and b_0 to b_{15} as $-\hbar^2/\left(2m(\Delta x)^2\right)$ multiplied by the following numbers (from left to right, then from top to bottom), respectively:

$-2 + 12.052110193235i$,	71.177637000065,	$262.693855125265i$,	708.598614518240,
$1461.844046849774i$,	2387.382683759241,	$3149.979100974855i$,	3395.091578678526,
$3000.639882589720i$,	2168.648792241722,	$1268.957016689205i$,	589.685213345064,
$210.491232766998i$,	54.442223074977,	$9.111658309311i$,	0.742160906401.

Now we present the boundary conditions based on ALEX [20]. First, we consider the left boundary $x = 0$. For $k < 0$, we directly take the boundary condition

$$i\hbar \frac{d}{dt}\psi_{0,l} = \sum_{q=0}^{M_q} b_q \psi_{q,l}. \tag{29}$$

For $k > 0$, we adopt the ALEX boundary condition for the reflected component $\psi_{j,l} - \exp(i(kx_j - \frac{E^d(k_l)}{\hbar}t))$. This gives for $j = 0$

$$i\hbar \frac{d}{dt}\psi_{0,l} = \sum_{q=0}^{M_q} b_q \psi_{q,l} + \exp\left(-i\frac{E^d(k_l)}{\hbar}t\right) E^d(k_l) - \exp\left(-i\frac{E^d(k_l)}{\hbar}t\right) \sum_{q=0}^{M_q} b_q \exp(ikq\Delta x). \tag{30}$$

Next, we consider the right boundary $x = L$. Using the transform

$$\tilde{\psi}_{j,l}(t) = \psi_{j,l}(t) \exp\left(-\frac{ie}{\hbar}\int_0^t U(s)ds\right), \tag{31}$$

one may show that $\tilde{\psi}_{j,l}$ is governed by the free discrete Schrödinger equation for $j \geq J$, namely, without the electric potential term. For $k < 0$, we adopt the ALEX boundary condition for the reflected part $\tilde{\psi}_{j,l} - \exp(i(kx_j - \frac{E^d(k)}{\hbar}t))$. Going back to $\psi_{j,l} = \tilde{\psi}_{j,l} \exp\left(\frac{ie}{\hbar}\int_0^t U(s)ds\right)$, we obtain the boundary condition

$$i\hbar \frac{d}{dt}\psi_{J,l} = \sum_{q=0}^{M_q} b_q \psi_{J-q,l} + V_J \psi_{J,l} + \exp\left(\frac{ie}{\hbar}\int_0^t U(s)ds - i\frac{E^d(k_l)}{\hbar}t\right)\left[E^d(k_l)\exp(ikL) - \sum_{q=0}^{M_q} b_q \exp(ik(L - q\Delta x))\right]. \tag{32}$$

For $k > 0$, the ALEX boundary condition for $\tilde{\psi}_{J,l}$ leads to

$$i\hbar \frac{d}{dt}\psi_{J,l} = \sum_{q=0}^{M_q} b_q \psi_{J-q,l} + V_J \psi_{J,l}. \tag{33}$$

3.3. Algorithm for the transient computation

We summarize advancing one step for the transient computation as follows. Let the wave function at a time $t^r \equiv r\Delta t$ be $\psi^r_{j,l}$ for $j = 0, \ldots, J$ and $|l| = 1, \ldots, M$.

Step 1 Evaluate the electron density n^r_j according to (23) for $j = 1, \ldots, J-1$;

Step 2 Solve the Poisson equation (22) by a standard solver to obtain the self-consistent electron potential energy and hence the total potential energy V^r_j for $j = 1, \ldots, J-1$;

Step 3 With the potential energy V^r_j, use the Crank-Nicolson scheme to solve the ordinary differential equation (24) at $j = 1, \ldots, J-1$ with the ALEX boundary conditions (29)-(33).

4. Numerical tests

We first present the stationary simulation of a resonant tunneling diode at zero applied voltage. Then we show the transient simulation results with initial data given by the stationary solution.

symbol	physical meaning	value
e	elementary charge	$1.602s10^{-19}$C
$\hbar$	reduced Planck constant	1.0546×10^{-34}J $\cdot$ s
m	effective mass	6.1033×10^{-32}kg
ε	permittivity	1.012319×10^{-10}F/m
k_B	Boltzmann constant	$1.3806505 \times 10^{-23}$J/K
E_F	Fermi energy	6.7097×10^{-21}J
T_0	semiconductor temperature	300K

Table 1: Physical constants and parameters in the simulation.

The physical constants used in this study are listed in Table 1. The electron doping profile is

$$n_D(x) = \begin{cases} 1 \times 10^{24}\text{m}^{-3}, & x \in [0, 50\text{nm}] \cup [85\text{nm}, 135\text{nm}], \\ 5 \times 10^{21}\text{m}^{-3}, & \text{elsewhere.} \end{cases} \tag{34}$$

The barrier potential is

$$V^B(x) = \begin{cases} 0.3\text{eV}, & x \in [60\text{nm}, 65\text{nm}] \cup [70\text{nm}, 75\text{nm}], \\ 0, & \text{elsewhere.} \end{cases} \tag{35}$$

They are schematically shown in Fig.1.

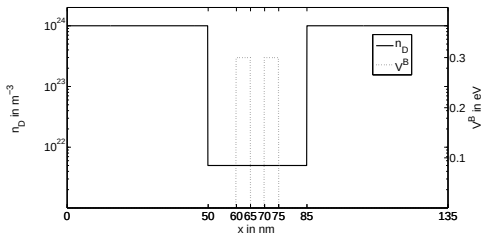

Figure 1: The doping profile and the given barrier potential energy.

We take $J = 1350$ and $M = 1500$. This yields $k_M = 6.26 \times 10^8\text{m}^{-1}$ as the cut-off wave number, according to the choice of physical constants and parameters.

4.1. Numerical solution of the stationary Schrödinger-Poisson system

For the stationary solution to the Schrödinger-Poisson system at zero applied voltage, Fig. 2 shows $|\varphi(x, k)|$ in the (x, k)-plane. A pair of peaks is clearly visible. They are located around $k \approx \pm 1174\Delta k$, and within the barrier region $[60\text{nm}, 75\text{nm}]$. See Fig.3. The peak's amplitude is 25.5385, much higher than elsewhere. They correspond to electrons trapped in the barrier, see Fig. 4. We call these peaks the *primary peaks*.

The conduction current density

$$J_{cond}(x) = \frac{e\hbar}{m} \int_{-k_M}^{k_M} g(k) Im\left(\varphi^*(x, k) \frac{\partial \varphi(x, k)}{\partial x}\right) dk, \tag{36}$$

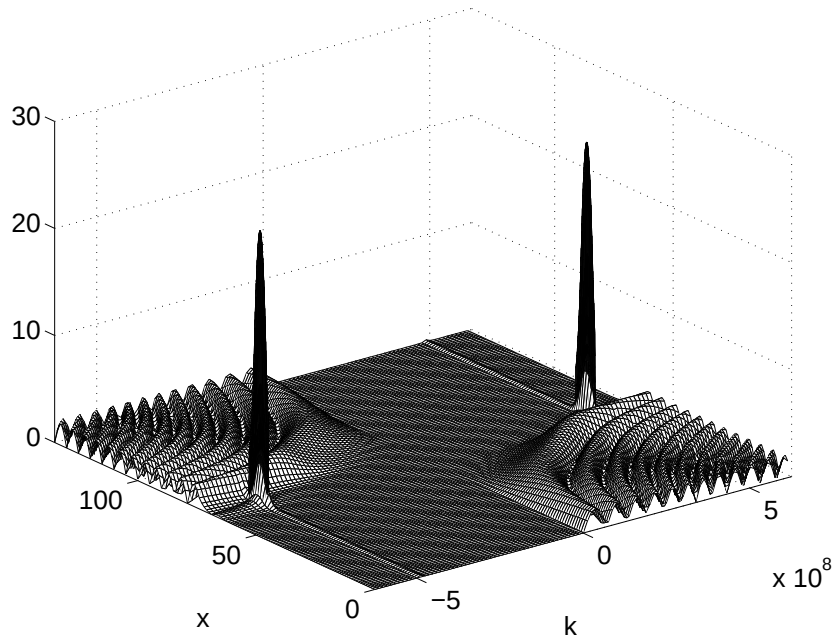

Figure 2: Wave function $|\varphi(x,k)|$ in the (x,k)-plane.

is depicted in Fig. 5. Noticing that the current density is on the order of $10^9\mathrm{A/m}^2$ when there is an applied voltage, this current density can practically be regarded as 0, as it is expected for zero applied voltage.

The self-consistent potential energy $\overline{V}^s$ is shown in Fig. 6. The doping profile, which is low for the depleted region $[50\mathrm{nm}, 85\mathrm{nm}]$, generates a hump there. The electron density variation around the double barrier does not lead to noticeable variation in the self-consistent potential energy. The difference between the electron density $\overline{n}(x)$ and the doping profile around the barrier is smaller than $5\times10^{22}\mathrm{m}^{-3}$. In contrast, around the doping profile edges this difference is on the order of $10^{24}\mathrm{m}^{-3}$.

4.2. Numerical solution of the transient Schrödinger-Poisson system

We solve the transient system with the ALEX boundary condition and the Crank-Nicolson scheme. The time step is chosen as $\Delta t = 0.5\mathrm{fs}$. The applied voltage is

$$U(t) = \begin{cases} \frac{U_0}{2}(1-\cos\frac{2\pi t}{T}), & 0 \le t \le 1\mathrm{ps}; \\ U_0, & t > 1\mathrm{ps}, \end{cases} \tag{37}$$

where $U_0 = 0.25\mathrm{V}$ and $T = 2\mathrm{ps}$.

First, we demonstrate that the proposed boundary treatments effectively suppress spurious reflections. In Fig. 7, we show the wave function modulus $|\psi(x,k,0.2\mathrm{ps})|$. As mentioned before, at the left boundary of the device ($x = 0$) there is no incoming wave for $k < 0$. The numerical

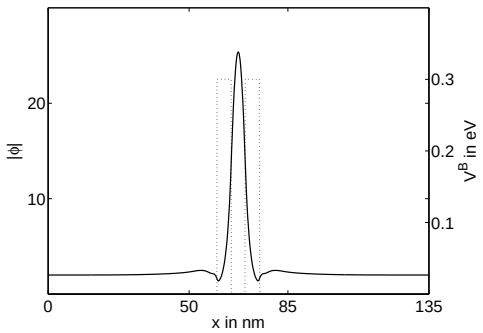

Figure 3: Wave function $|\varphi(x,k)|$: a "side view" ($\max_k |\varphi(x,k)|$).

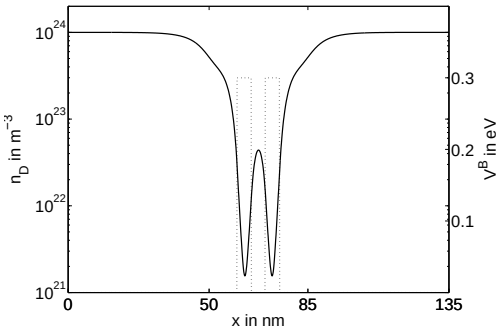

Figure 4: The electron density $\overline{n}(x)$.

solution does not show any spurious reflection. Similarly, no reflection is observed at the right boundary ($x = 135$nm) for $k > 0$. In Fig. 7, the tails of the two primary peaks (at $k = \pm 1174\Delta k$) show some oscillations that extend up to the outflow boundary. They are due to the transient evolution of the wave function and are *not* caused by the boundary treatment. This was confirmed by simulations on a larger spatial domain. In Fig. 8, we compare the wave function modulus at the resonant wave number $1174\Delta k$ and time $t = 0.2$ps with a reference solution calculated with an extended domain $x \in [0, 2L]$. The excellent agreement illustrates the effectiveness of the proposed ALEX boundary conditions. We also note that these oscillations do not present in the stationary simulation shown in Fig. 2. Moreover, the primary peaks remain at the same (x,k)-position, compared to the zero-bias case at $t = 0$, see Fig. 2. Yet their amplitudes decrease slightly to 25.3392. The change in wave function modulus is shown in Fig.9. The biggest change occurs along $\pm 1174\Delta k$. We remark that while the change in $|\psi|$ is moderate, a significant phase difference during the evolution makes the change in ψ itself rather large.

To check the effectiveness of the boundary treatment in more detail, we focus on a particular wave number $k = \Delta k$, and plot the evolution of the wave function modulus $|\psi(x,k,t)|$ for $t \in [0, 0.2\text{ps}]$ in the upper-left subplot of Fig. 10. In the upper-right plot, we zoom in the right-boundary vicinity $x \in [130\text{nm}, 135\text{nm}]$. The directions of contour lines clearly demonstrate that the wave propagates from left to right as time elapses, without observable reflections. For the left

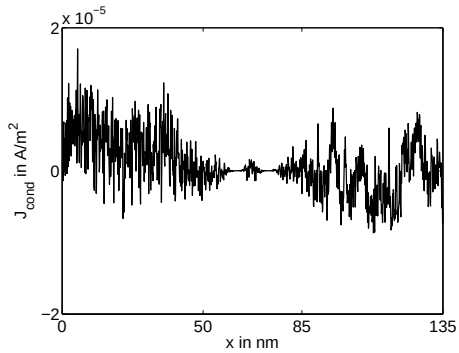

Figure 5: Current density in the stationary Schrödinger-Poisson system.

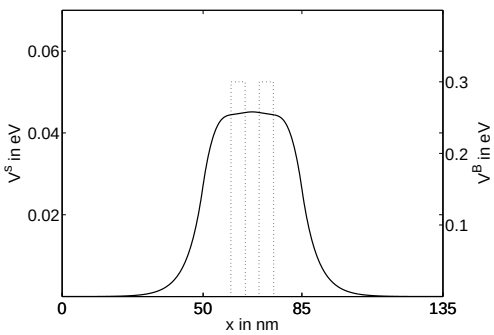

Figure 6: Self-consistent potential energy in the stationary Schrödinger-Poisson system.

boundary vicinity $x \in [0\text{nm}, 5\text{nm}]$ in the lower-left subplot, the wave function consists of both an incoming part, and the rest that comes from wave propagation and complex dynamics. In the lower-right subplot, we show that the mentioned rest is indeed an outgoing wave that propagates from right to left.

With the numerical boundary treatment validated, we now briefly describe the behavior of the device, which agrees with those in the literature [10][11][12]. As seen from Fig. 7, the peaks persist over the whole simulation time, yet this amplitude varies. The evolution in the wave function leads to a change in the electron density, current and self-consistent potential.

From Fig.11, we observe that, when the applied voltage increases from 0 to $\frac{U_0}{2}$ at $t = 0.5$ps, the electron density increases in the left barrier and the intermediate region between the two barriers, which clearly reflects the resonant tunnelling mechanism. The electron density inside the right barrier does not change much, and to the right of it, it decreases considerably. Accordingly, the conduction current increases in this period. Afterwards, when the applied voltage further increases up to U_0 at $t = 1$ps, the electron density moves up in the left barrier and the intermediate region. The conduction current density also moves up accordingly. However, at the left doping gradient boundary, a minor kink develops at about $x = 52$nm. This may mean that there are not enough electrons from the right side, yet the increment in applied voltage attracts more electrons to the left. The conduction current density moves downward away from the barriers,

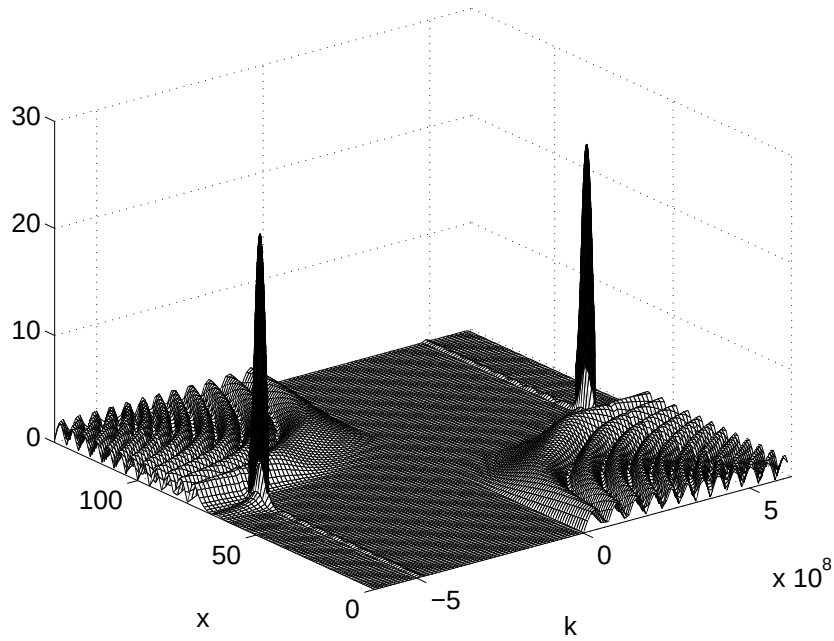

Figure 7: Wave function $|\psi(x, k, 0.2\text{ps})|$.

leading to a smaller total current. After $t = 1$ps, when the applied voltage remains at U_0, there are more electrons accumulated in the intermediate region, and the conduction current density profile becomes flatter in the device.

In Fig. 12, we plot the total current density averaged over $[0, L]$ during the whole time period, which is defined as

$$J_{total} = J_{cond} - \frac{\varepsilon}{e}\frac{\partial}{\partial t}\nabla V^s. \tag{38}$$

This agrees with [1]. If we take the discrete transparent boundary conditions with the exact convolution from [14][1] as the reference solution, we observe that the numerical error in our solution is negligible, cf. Fig. 13. Defining the relative L^2-error as

$$\varepsilon_r(t) = \frac{\sqrt{\int_0^L (J_{cond}(x,t) - J_{cond}^{ref}(x,t))^2 dx}}{\sqrt{\int_0^L (J_{cond}^{ref}(x,t))^2 dx}}, \tag{39}$$

we obtain $\varepsilon_r(1.5\text{ps}) = 6.45 \times 10^{-10}$.

In Fig. 13, we also present the current density $J_{cond}(x, 1.5\text{ps})$ computed with approximate discrete transparent boundary conditions for a fast evaluation of the convolutions (as developed in [17] and used in [1]). There the exact convolution kernel is approximated by a sum of Λ (discrete) exponential terms. Fig. 13 gives the results for $\Lambda = 10$ and 20. But even when $\Lambda = 100$ (cf. Fig. 11 in [1]) yields a larger error than our ALEX boundary treatment. This demonstrates the effectiveness of our boundary treatment.

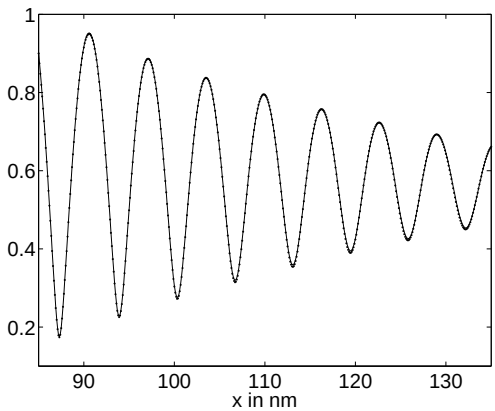

Figure 8: Comparison in wave function modulus $|\psi(x, 1174\Delta k, 0.2\text{ps})|$: solid line for reference solution, and dots for numerical solution.

5. Primary peaks

The primary peaks of $|\varphi(x, k)|$ are prominent in the wave function profile of a resonant tunneling diode. They are induced by the double barrier structure, and influence the physics in the device.

To better understand these peaks, we first double the computational domain in wave number space, namely, $k \in [-3000\Delta k, 3000\Delta k]$. As shown in Fig. 14 for the stationary Schrödinger-Poisson simulation, a pair of secondary peaks appears at $k \approx \pm 1866\Delta k$, with a much smaller amplitude. Because of the fast decay in the Fermi-Dirac distribution (9), the extended computational domain, and in particular the secondary peaks do not lead to a significant change in the electron density n or the potential energy V. Moreover, it is observed that the secondary peaks are at an energy level equal to the barrier potential, namely,

$$\frac{\hbar^2 k^2}{2m} = e(V^B + \overline{V}^s) = 5.5269 \times 10^{-20}\text{J}. \tag{40}$$

Note that wave numbers k (or injection energies) below the level of the barrier potential make the transmission close to zero (except for the primary peaks $k \approx \pm 1174\Delta k$). Consider $\varphi(0, k < 0) \approx 0$ and $\varphi(L, k > 0) \approx 0$ in Fig. 2 and Fig. 14. For higher injection energies, however, the modulus of the transmission coefficient is close to 1. Consider $|\varphi(0, k < -1866\Delta k)| \approx 1$ and $|\varphi(L, k > 1866\Delta k)| \approx 1$ in Fig. 14. We remark that in the classical limit, the modulus of the transmission coefficient would jump from 0 to 1 at wave numbers corresponding to the barrier height.

To further explore the choice of the wave number domain, we calculate the electron density $\overline{n}_j$ with different cut-off wave numbers. In analogy to the partial sum in (18), we consider now

$$\overline{n}_j^M \equiv \Delta k \sum_{|l|=1}^{M} g(k_l)|\varphi_{j,l}|^2, \tag{41}$$

for some fixed values of j. Fig.15 shows $\overline{n}_j^M$ as a function of M. For the positions $x \leq 60$nm (and by symmetry also for $x \geq 75$nm), the function $\overline{n}_j^M$ almost saturates for $M = 800$. But for the

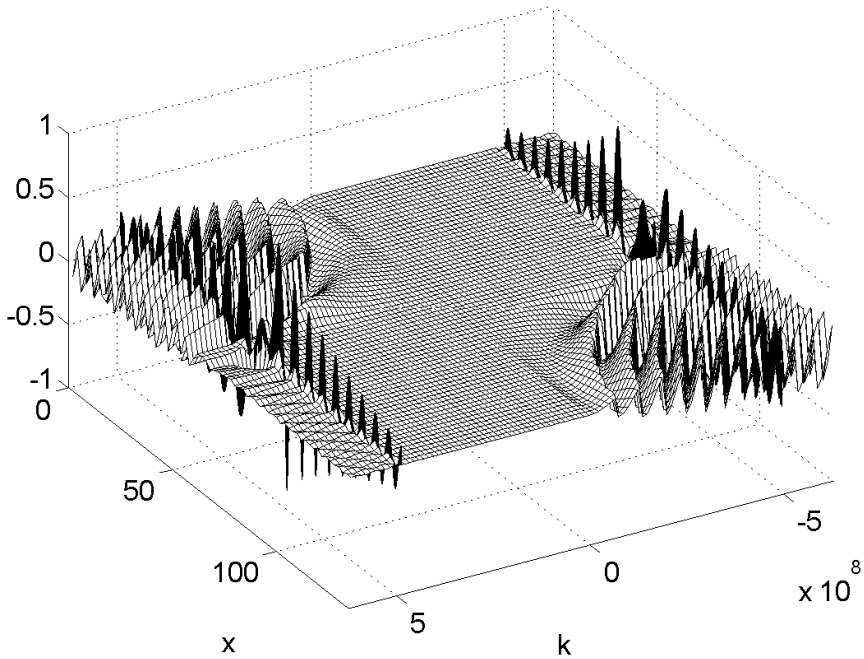

Figure 9: Change in wave function modulus $|\psi(x, k, 0.2\text{ps})| - |\psi(x, k, 0\text{ps})|$.

positions $62.5nm \leq x \leq 67.5\text{nm}$, $\overline{n}_j^M$ has a significant jump close to $M = 1174$. This explains that the choice of $k_M = \sqrt{2m(E_F + 7k_BT_0)}/\hbar$ is sufficient in (9) for 0 applied voltage. In Fig. 4, we plotted the electron density for summation over the whole computational domain (with respect to the wave number). The hump inside the barrier is caused by the two peaks, as explained above.

The primary peaks may be explained as a resonance phenomenon in the quantum device. But the computation of their location in k-space via the nonlinear stationary Schrödinger system is costly. Hence we shall now present a semi-heuristic linear model to simplify that computation. Inspired by V^s from Fig. 6, we shall use now the approximate self-consistent potential $\tilde{V}^s(x) = 0.045\text{eV} \cdot \chi_{[60\text{nm},75\text{nm}]}(x)$. This leads to the following stationary Schrödinger equation

$$E(k)\phi = -\frac{\hbar^2}{2m}\phi_{xx} + V(x)\phi, \quad x \in \mathbb{R}, \tag{42}$$

with the total potential

$$V(x) = \begin{cases} 0, & x < 60\text{nm}; \\ 0.345\text{eV}, & 60\text{nm} < x < 65\text{nm}; \\ 0.045\text{eV}, & 65\text{nm} < x < 70\text{nm}; \\ 0.345\text{eV}, & 70\text{nm} < x < 75\text{nm}; \\ 0, & x > 75\text{nm}. \end{cases} \tag{43}$$

We rescale $V(x)$ by 0.345eV, shift x by 67.5nm and rescale it by $\hbar/\sqrt{2m \cdot 0.345\text{eV}}$, and rescale k by $\sqrt{2m \cdot 0.345\text{eV}}/\hbar$. Let $w \equiv 2.5\text{nm}/[\hbar/\sqrt{2m \cdot 0.345\text{eV}}] = 1.9471096$, $\eta \equiv 0.045\text{eV}/0.345\text{eV} =$

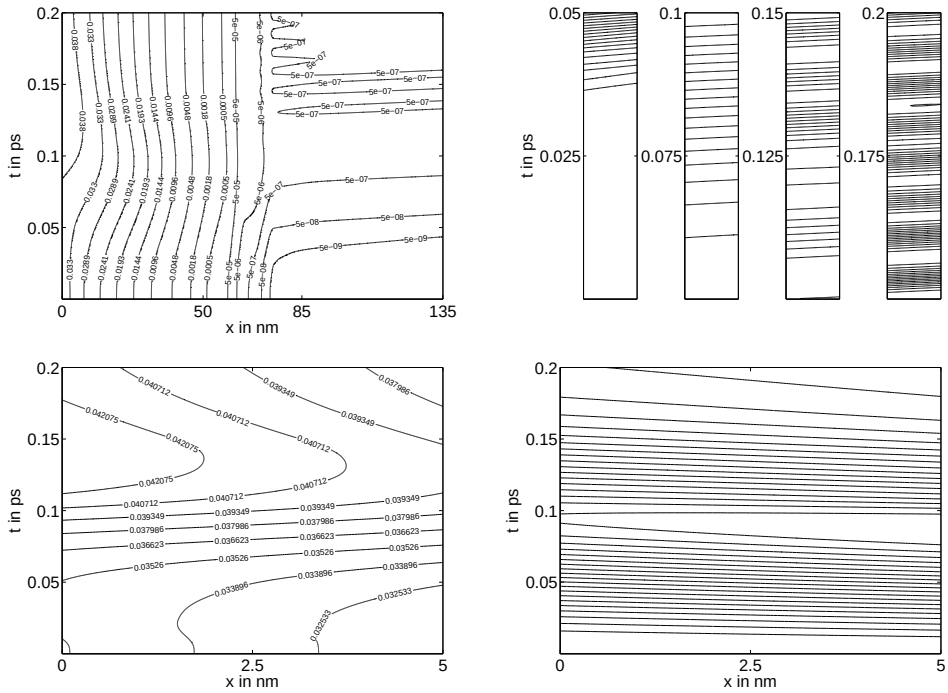

Figure 10: $|\psi(x, \Delta k, t)|$ for $t \in [0, 0.2\text{ps}]$. Upper-left: wave function in the whole device; upper-right: blow-up view near the right boundary for $x \in [130\text{nm}, 135\text{nm}]$, time $t \in [0, 0.2\text{ps}]$ in four equal length t-intervals; lower-left: blow-up view near the left boundary for $x \in [0, 5\text{nm}]$; lower-right: $\left|\psi(x, \Delta k, t) - \exp\left(-iE^d(\Delta k)/\hbar t + i\Delta k x\right)\right|$ near the left boundary for $x \in [0, 5\text{nm}]$.

0.1304348. Then the rescaled equation and potential are as follows:

$$E(k)\phi = -\phi_{xx} + V(x)\phi, \quad x \in \mathbb{R}, \tag{44}$$

$$V(x) = \begin{cases} 0, & x < -3w; \\ 1, & -3w < x < -w; \\ \eta, & -w < x < w; \\ 1, & w < x < 3w; \\ 0, & x > 3w. \end{cases} \tag{45}$$

Further let $\alpha \equiv \sqrt{1-k^2}$ and $\beta \equiv \sqrt{k^2-\eta}$. The analytical solution of (44)-(45) with an incident wave $\exp(ikx)$ from the left with $\sqrt{\eta} < k < 1$ takes the following form

$$\phi(x,k) = \begin{cases} \exp(ikx) + R(k)\exp(-ikx), & x < -3w; \\ A_-\exp(\alpha x) + B_-\exp(-\alpha x), & -3w < x < -w; \\ A_0\exp(i\beta x) + B_0\exp(-i\beta x), & -w < x < w; \\ A_+\exp(\alpha x) + B_+\exp(-\alpha x), & w < x < 3w; \\ T(k)\exp(ikx), & x > 3w. \end{cases} \tag{46}$$

Here the matching coefficients $A_-, A_0, A_+, B_-, B_0, B_+$ are to be determined. $R(k)$ and $T(k)$ are reflection and transmission coefficients, respectively. Making use of $\phi(x) \in C^1$, we may form a linear algebraic system for the above coefficients. Eliminating the matching coefficients, we end up with

$$\begin{bmatrix} T(k)\exp(3ikw) \\ 0 \end{bmatrix} = -\frac{1}{16\alpha^2\beta k}\begin{bmatrix} \alpha+ik & -\alpha+ik \\ -\alpha+ik & \alpha+ik \end{bmatrix}\Lambda(2\alpha)\begin{bmatrix} \alpha+i\beta & \alpha-i\beta \\ \alpha-i\beta & \alpha+i\beta \end{bmatrix}\Lambda(2i\beta)$$
$$\cdot\begin{bmatrix} \alpha+i\beta & -\alpha+i\beta \\ -\alpha+i\beta & \alpha+i\beta \end{bmatrix}\Lambda(2\alpha)\begin{bmatrix} \alpha+ik & \alpha-ik \\ \alpha-ik & \alpha+ik \end{bmatrix}\Lambda(-3ik)\begin{bmatrix} 1 \\ R(k) \end{bmatrix}, \tag{47}$$

with the diagonal matrix

$$\Lambda(s) = \begin{bmatrix} \exp(sw) & 0 \\ 0 & \exp(-sw) \end{bmatrix}.$$

Solving this linear system for R and T, we find that resonance, i.e., $|T(k)| = 1$ occurs at about $k^* = 0.62458$. This gives, in physical units, a wave number of $0.62458 \times \sqrt{2m \cdot 0.345\text{eV}}/\hbar = 4.8645 \times 10^8\text{m}^{-1}$. In our stationary solution from Section 4.1, the primary peaks appear at $1174\Delta k = 4.8995 \times 10^9\text{m}^{-1}$. Hence, the relative error from the simplified linear model (44)-(45) is less than 1%. Numerically, the transmission and reflection coefficients are $|T(k^*)| = 0.999972, |R(k^*)| = 0.007418$. Moreover, the maximal amplitude of $|\phi(x, k^*)| = 24.5175$ at $x = 0$. Again it agrees well with the full stationary Schrödinger-Poisson simulation, which gives 25.5385, see Fig. 16.

With the above discussions, we propose to prescribe the cut-off wave number in a new way, namely, $\tilde{k}_M \equiv \max\left(\sqrt{2m(E_F + 7k_BT_0)}/\hbar, \sqrt{2m \cdot \max V^B(x)}/\hbar\right)$, where the second term corresponds to the level of the potential barrier. Under the settings described before, this amounts to $7.26 \times 10^8\text{m}^{-1}$.

6. Conclusion

In this paper, we propose the ALEX boundary treatment to effectively suppress spurious reflections in the wave functions at the ends of the resonant-tunneling diode device. It yields high accuracy, comparable to the theoretically exact boundary treatment developed in [16] and applied in [1]. The numerical cost and programming complexity are reduced considerably. Being local in both space and time, it bears nice features of being simple, clear, and without empirical parameters. When the mesh size or time step size changes during a simulation, it is not necessary to restart the simulation from the beginning, in contrast to the time history dependent boundary treatments in [1]. The numerical results with the proposed ALEX boundary treatments demonstrate the effectiveness.

In the wave function profile, we observe two primary peaks around $\pm 1174\Delta k$, located inside the barrier potential well in space. With the choice of cut-off wave number proposed in previous works [15][1], these peaks are included in the computational domain. The important role of the primary peaks is revealed by a careful study of the partial sums in calculating the electron density. In addition, when a bias is applied, the biggest change in wave function profile is at the corresponding resonant wave numbers $k_{res} \approx 4.8995 \times 10^9\text{m}^{-1}$. Accordingly, the cut-off wave number *must* be determined so that the primary peaks are included in the simulation domain. Moreover, the position and amplitude of the peaks are accurately modeled by a simplified model at zero applied voltage.

Acknowledgement

This study is partially supported by the National Natural Science Foundation of China under contract numbers 11272009 and 11521202. Anton Arnold was supported by the FWF-Doctoral School W1245. The authors would like to thank Prof. Jüngel for providing the electronic file of the current density at $t = 1.5$ps, and the anonymous referees for helpful improvements of the manuscript.

References

[1] J.-F. Mennemann, A. Jüngel, H. Kosina, Transient Schrödinger–Poisson simulations of a high-frequency resonant tunneling diode oscillator, Journal of Computational Physics 239 (2013) 187–205.
[2] C. Bardos, L. Erdös, F. Golse, N. Mauser, H.-T. Yau, Derivation of the Schrödinger-Poisson equation from the quantum N-body problem, Comptes Rendus Mathematique 334 (2002) 515–520.
[3] M. A. Marques, E. Gross, Time-dependent density functional theory, Annual Review of Physical Chemistry 55 (2004) 427–455.
[4] B. Mayfield, Non–local boundary conditions for the Schrödinger equation, Ph.D. thesis, University of Rhode Island, Providence, RI, 1989.
[5] V. Baskakov, A. Popov, Implementation of transparent boundaries for numerical solution of the Schrödinger equation, Wave Motion 14 (1991) 123–128.
[6] N. Ben Abdallah, S. Tang, On hybrid quantum–classical transport models, Mathematical Methods in the Applied Sciences 27 (2004) 643–667.
[7] J.-F. Mennemann, A. Jüngel, Perfectly matched layers versus discrete transparent boundary conditions in quantum device simulations, Journal of Computational Physics 275 (2014) 1–24.
[8] X. Antoine, A. Arnold, C. Besse, M. Ehrhardt, A. Schädle, A review of transparent and artificial boundary conditions techniques for linear and nonlinear Schrödinger equations, Communications in Computational Physics 4 (2008) 729–796.
[9] G. Pang, S. Tang, Approximate linear relations for Bessel functions, preprint (2015).
[10] G. Pang, L. Bian, S. Tang, Almost exact boundary condition for one-dimensional Schrödinger equations, Physical Review E 86 (2012) 066709.
[11] A. Jüngel, S. Tang, Numerical approximation of the viscous quantum hydrodynamic model for semiconductors, Applied Numerical Mathematics 56 (2006) 899–915.
[12] X. Hu, S. Tang, Transient and stationary simulations for a quantum hydrodynamic model, Chinese Physics Letters 24 (2007) 1437.
[13] N. B. Abdallah, P. Degond, P. A. Markowich, On a one-dimensional Schrödinger-Poisson scattering model, Zeitschrift für angewandte Mathematik und Physik ZAMP 48 (1997) 135–155.
[14] A. Arnold, Mathematical concepts of open quantum boundary conditions, Transport Theory and Statistical Physics 30 (2001) 561–584.
[15] N. B. Abdallah, A. Faraj, An improved transient algorithm for resonant tunneling, arXiv preprint arXiv:1005.0444 (2010).
[16] A. Arnold, Numerically absorbing boundary conditions for quantum evolution equations, VLSI Design 6 (1998) 313–319.
[17] A. Arnold, M. Ehrhardt, I. Sofronov, Discrete transparent boundary conditions for the Schrödinger equation: Fast calculation, approximation, and stability, Communications in Mathematical Sciences 1 (2003) 501–556.
[18] X. Antoine, C. Besse, Unconditionally stable discretization schemes of non-reflecting boundary conditions for the one-dimensional Schrödinger equation, Journal of Computational Physics 188 (2003) 157–175.
[19] C. Zheng, A perfectly matched layer approach to the nonlinear Schrödinger wave equations, Journal of Computational Physics 227 (2007) 537–556.
[20] S. Tang, A two-way interfacial condition for lattice simulations, Advances in Applied Mathematics and Mechanics 2 (2010) 45–55.

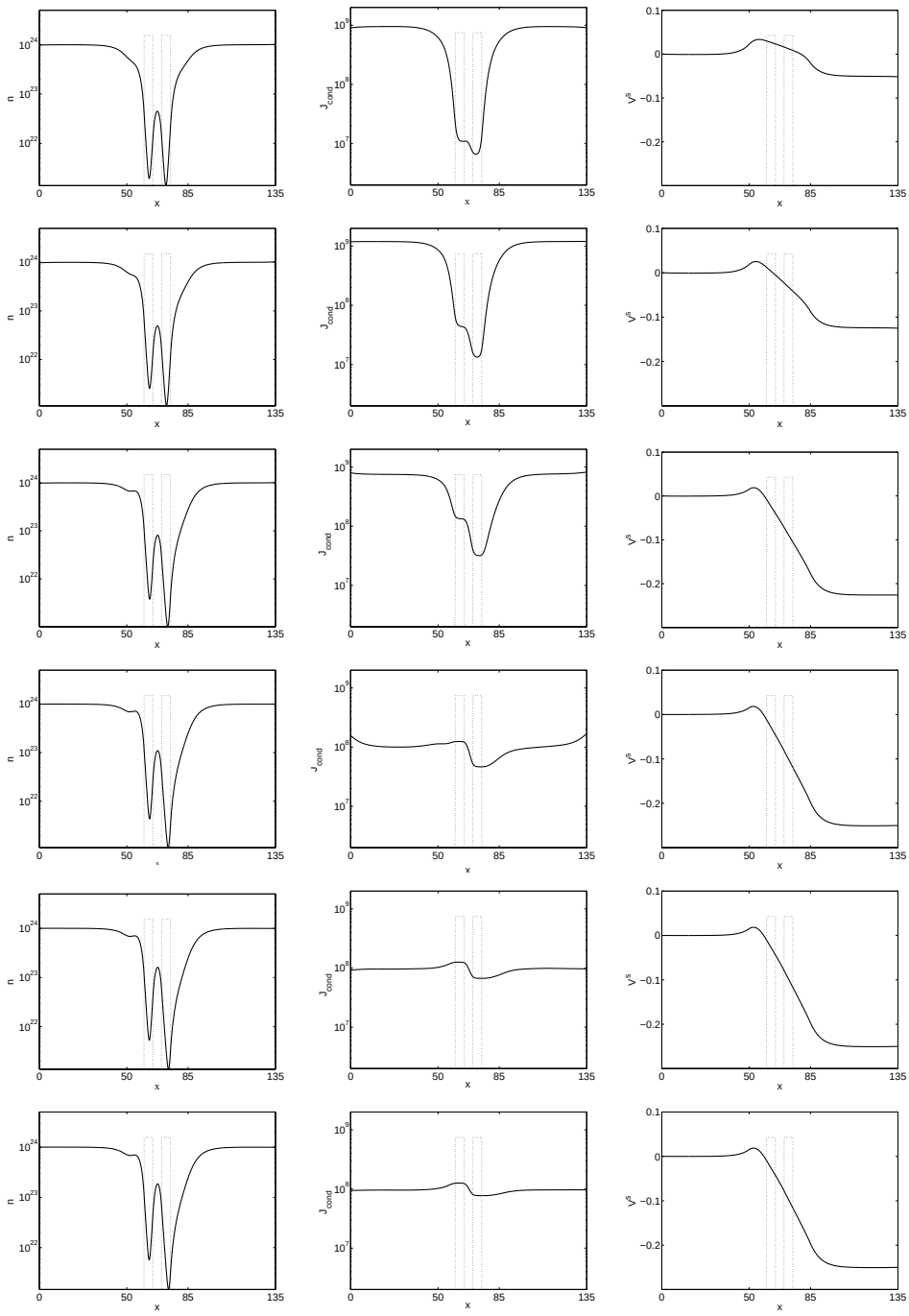

Figure 11: Left column: electron density in m^{-3}; middle column: current density in A/m^2; right column: self-consistent potential energy in eV. Different rows show different times: t =0.3ps, 0.5ps, 0.8ps, 1.0ps, 1.5ps and 2.0ps (top to bottom), respectively.

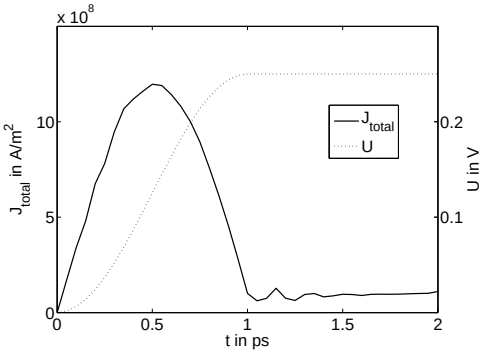

Figure 12: Solid line: total current density as a function of *t*, averaged in space. Dotted line: applied bias as a function of *t*.

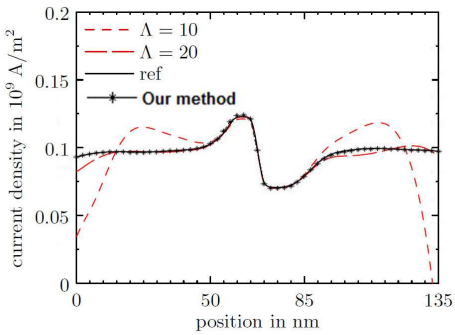

Figure 13: Conduction current density at t = 1.5ps with comparison to [1].

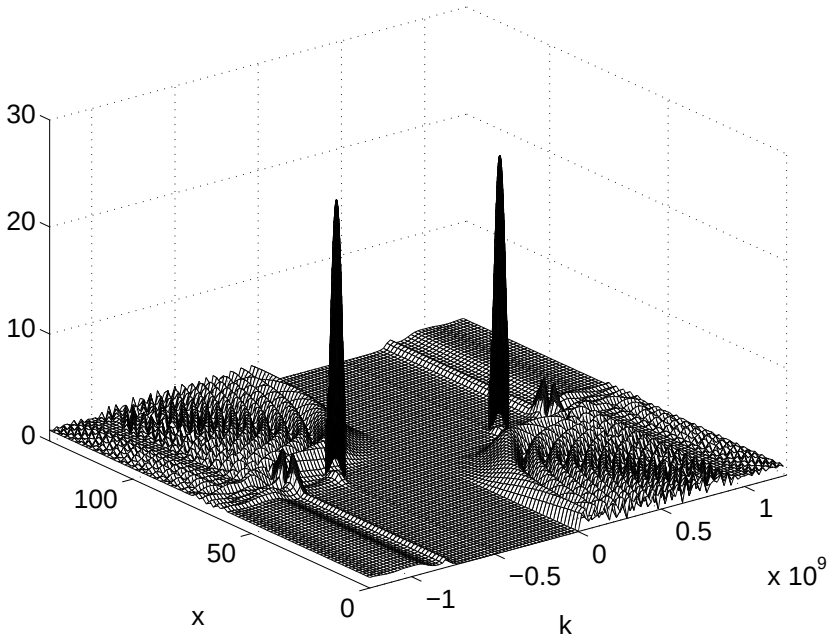

Figure 14: Wave function $|\varphi(x, k)|$ computed with cut-off wave number $k'_M = 2k_M$.

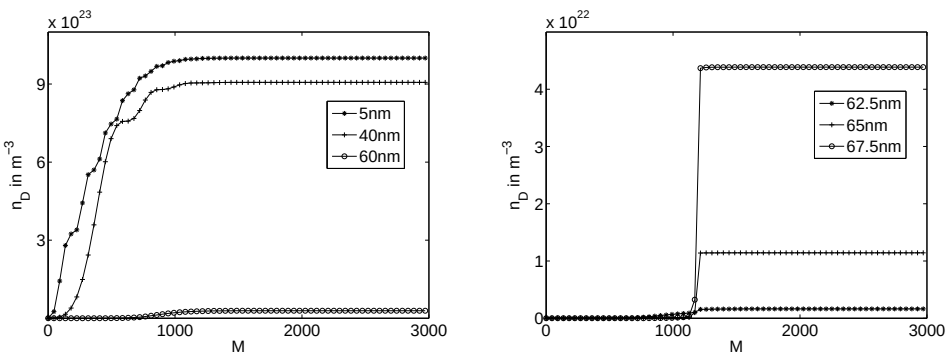

Figure 15: Partial sum for the electron density $\overline{n}_j^M$ as a function of M. The results are given for six values of $x_j = j\Delta x$.

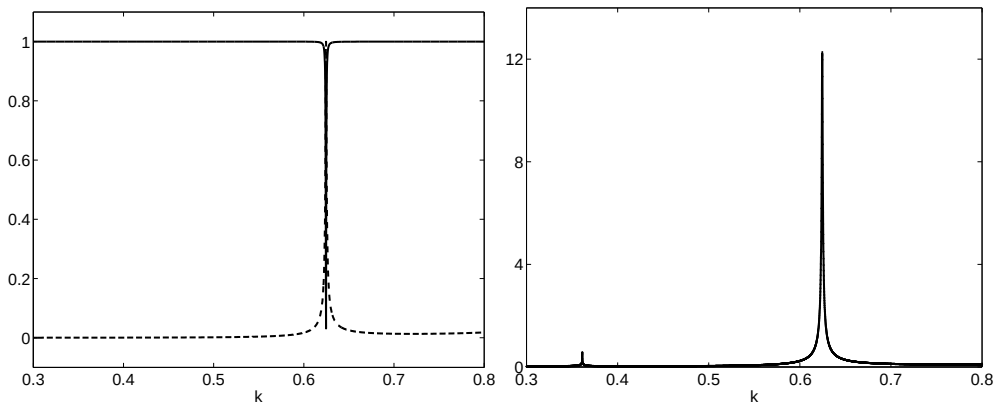

Figure 16: Resonance computed with the simplified model. Left: reflection coefficient $|R(k)|$ (solid line) and transmission coefficient $|T(k)|$ (dashed line) as function of k. Right: matching coefficients $|A_0|$ (solid line) and $|B_0|$ (dashed line) from (46), which coincide with each other. They represent the amplitude of the two traveling waves inside the potential barriers. The horizontal axis stands for the undimensionalized wave number k.